

Learning of feature points without additional supervision improves reinforcement learning from images

Rinu Boney, Alexander Ilin, Juho Kannala

Department of Computer Science
Aalto University, Finland
firstname.lastname@aalto.fi

Abstract

In many control problems that include vision, optimal controls can be inferred from the location of the objects in the scene. This information can be represented using feature points, which is a list of spatial locations in learned feature maps of an input image. Previous works show that feature points learned using unsupervised pre-training or human supervision can provide good features for control tasks. In this paper, we show that it is possible to learn efficient feature point representations end-to-end, without the need for unsupervised pre-training, decoders, or additional losses. Our proposed architecture consists of a differentiable feature point extractor that feeds the coordinates of the estimated feature points directly to a soft actor-critic agent. The proposed algorithm yields performance competitive to the state-of-the art on DeepMind Control Suite tasks.

Introduction

Learning state representations of image observations for control is highly challenging as images are high-dimensional and supervisory signals in reinforcement learning (RL) are limited to scalar rewards. State-of-the-art model-free RL algorithms with convolutional encoders, without any additional enhancements, have been highly data-inefficient in this setting (Tassa et al. 2020; Yarats et al. 2019). A popular solution is to enhance the supervision of the encoder by introducing an auxiliary autoencoding task (Yarats et al. 2019). Another popular approach is contrastive representation learning in which there is an auxiliary task of selecting a matching representation (obtained for another transformation of the same input) among a number of alternatives (Laskin, Srinivas, and Abbeel 2020). More recently, image augmentations such as small random shifts have been found to enable data-efficient RL from images without any additional auxiliary loss functions (Laskin et al. 2020; Yarats, Kostrikov, and Fergus 2021).

In this work, we represent the state of an actor-critic RL agent using a small set of “feature points” extracted from high-dimensional image inputs. Feature points can be seen as spatial locations of features in the input image which are useful for the task at hand. Feature points could represent the locations of objects or object parts, or spatial relations between objects. For example, a feature point located between two object locations could track their relative motion.

The motivation for using this type of representation is the intuition that the information in images consists of the appearance and geometry of the objects in the scene. Auxiliary tasks like autoencoding force the encoder to represent both types of information. However, what matters in many control problems is the geometry of the objects in the scene, not their exact appearance. Therefore, extracting the geometry information while neglecting the appearance information might lead towards better state representations.

We use a simple feature point bottleneck on top of a convolutional encoder and train it end-to-end with an actor-critic algorithm, without any pre-training or additional supervision. Our approach, which we term as FPAC (feature point actor-critic), is robust to a different number of objects and object dynamics. While a convolutional encoder trained with the Soft Actor-Critic (SAC) algorithm (Haarnoja et al. 2018a,b) is highly data-inefficient, the simple addition of a feature point bottleneck in FPAC greatly improves the learning performance, to attain data-efficiency and asymptotic performance competitive to state-of-the-art methods. The code to reproduce our FPAC experiments is available at <https://github.com/rinuboney/FPAC>.

Related Work

Our work is closely related to prior works (Levine et al. 2016; Finn et al. 2016; Cabi et al. 2020) which learn feature points for continuous control from images. Levine et al. (2016); Finn et al. (2016) train a non-linear neural policy with an intermediate feature point representation using supervised learning to imitate a local linear-Gaussian controller. We use a similar architecture of the neural policy with a differential feature point bottleneck. While (Levine et al. 2016) assume access to the ground truth low-dimensional state of the environment, we directly learn the control policy from pixels by feeding the extracted feature point representations to an actor-critic algorithm. Cabi et al. (2020) learn feature points for batch reinforcement learning but rely on human demonstrations and manual reward annotation. We perform a study of feature point learning on popular continuous control tasks to show that it improves reinforcement learning from images, without any additional supervision, even in tasks with sparse rewards.

The feature point bottleneck mechanism proposed in (Levine et al. 2016) has been used for unsupervised rep-

resentation learning in several works. The works of (Finn et al. 2016; Jakab et al. 2018; Zhang et al. 2018) use it an auto-encoding framework to learn feature points in an unsupervised manner based on image generation. Kulkarni et al. (2019) improved upon this by introducing a feature-transport mechanism to learn feature points that are more spatially aligned. Recently, Gopalakrishnan, van Steenkiste, and Schmidhuber (2021) proposed to learn object feature points based on local spatial predictability of image regions. Both (Kulkarni et al. 2019) and (Gopalakrishnan, van Steenkiste, and Schmidhuber 2021) demonstrate that feature points extracted using a pre-trained encoder serve as an effective state representation in some Atari games. We consider continuous control tasks and observe that pre-trained feature points fail to generalize well in some tasks while feature points learned end-to-end with RL perform better (see Fig. 2). Minderer et al. (2019) learn stochastic feature point dynamics models in an unsupervised manner and demonstrate their efficacy on reward prediction in some continuous control tasks. Manuelli et al. (2020) trained dense image descriptions using self-supervised correspondence to extract keypoints and learn keypoint dynamics models for model-based control in real-world robotic manipulation. While these prior works use generic tasks like image generation (Jakab et al. 2018; Zhang et al. 2018; Kulkarni et al. 2019; Gopalakrishnan, van Steenkiste, and Schmidhuber 2021) or equivariance constraints (Thewlis, Bilen, and Vedaldi 2017; Zhang et al. 2018; Thewlis et al. 2019) to learn feature points in an unsupervised manner, we aim to directly learn feature points that are relevant for control. We do not use any additional auxiliary losses that are specific to feature point learning but instead rely on end-to-end learning with RL losses to learn feature points that are well-aligned for the control task at hand.

Any unsupervised visual representation learning method could be used to potentially improve RL from images. Compressing high-dimensional image observations using a pre-trained autoencoder to assist RL was first proposed in (Lange and Riedmiller 2010) and later improved in other works (Yarats et al. 2019; Shelhamer et al. 2016; Higgins et al. 2017; Nair et al. 2018). Stable RL from images without any additional loss functions was demonstrated using the DDPG algorithm in (Tassa et al. 2020) using only the critic loss to update the convolutional encoder. Yarats et al. (2019) jointly trained a regularized convolutional autoencoder with the SAC algorithm. Laskin, Srinivas, and Abbeel (2020) trained the convolutional encoder jointly using the SAC algorithm and an unsupervised contrastive loss function. Recently, Laskin et al. (2020) and Yarats, Kostrikov, and Fergus (2021) concurrently discovered that some image augmentations such as small random shifts enable data-efficient RL on image-based RL benchmarks, without any additional auxiliary loss functions. Learned latent dynamics models have also been successfully used for planning (Hafner et al. 2019b) or to assist policy search (Hafner et al. 2019a; Ha and Schmidhuber 2018) for continuous control from images. These methods have been also successfully used to demonstrate data-efficient RL in some real-world robot tasks (Singh et al. 2019; Zhu et al. 2019; Kendall et al.

2019; Viitala et al. 2020). In this paper, we aim to improve sample-efficiency of RL by learning feature points that distill the geometric information from images.

Reinforcement Learning

We formulate continuous control from images as a Markov decision process (MDP). An MDP consists of a set of states \mathcal{S} , a set of actions \mathcal{A} , a transition probability function $\mathbf{s}_{t+1} \sim p(\cdot | \mathbf{s}_t, \mathbf{a}_t)$ that represents the probability of transitioning to a state \mathbf{s}_{t+1} by taking action \mathbf{a}_t in state \mathbf{s}_t at timestep t , a reward function $r_t = R(\mathbf{s}_t, \mathbf{a}_t)$ that provides a scalar reward for taking action \mathbf{a}_t in state \mathbf{s}_t , and a discount factor $\gamma \in [0, 1]$ to weigh future rewards.

The policy function $\mathbf{a}_t \sim \pi(\cdot | \mathbf{s}_t)$ of an RL agent defines the behavior of the agent: it is a mapping from the state to actions. The goal in RL is to learn a policy function π that maximizes the expected cumulative reward given by

$$\mathbb{E}_{\mathbf{s}_{t+1} \sim p(\cdot | \mathbf{s}_t, \mathbf{a}_t), \mathbf{a}_t \sim \pi(\mathbf{s}_t)} \left[\sum_{t=0}^{\infty} \gamma^t R(\mathbf{s}_t, \mathbf{a}_t) \right], \forall \mathbf{s}_0 \in \mathcal{S}.$$

In this paper, we solve the RL problem using the state-of-the-art Soft Actor-Critic (SAC) algorithm (Haarnoja et al. 2018b). SAC contains an actor network which produces stochastic policy π and a critic network which implements the state-action value function $Q^\pi(\mathbf{s}, \mathbf{a})$, which is the expected cumulative reward after taking action \mathbf{a} in state \mathbf{s} and following π thereafter. The policy π is tuned to maximize an entropy-regularized RL objective $\mathbb{E}[\sum_{t=0}^{\infty} \gamma^t (R(\mathbf{s}_t, \mathbf{a}_t) + \alpha \mathcal{H}(\pi(\cdot | \mathbf{s}_t)))]$, where $\alpha > 0$ is a learnable temperature parameter. The critic network Q is trained to satisfy the Bellman equation: $Q^\pi(\mathbf{s}_t, \mathbf{a}_t) = r_t + \gamma Q^\pi(\mathbf{s}_{t+1}, \pi(\mathbf{s}_{t+1}))$. It is updated by sampling transitions $(\mathbf{s}_t, \mathbf{a}_t, r_t, \mathbf{s}_{t+1})$ from a replay buffer \mathcal{D} and minimizing the critic loss

$$J_Q = \mathbb{E}_{(\mathbf{s}_t, \mathbf{a}_t, r_t, \mathbf{s}_{t+1}) \sim \mathcal{D}} [(Q(\mathbf{s}_t, \mathbf{a}_t) - r_t - \gamma V(\mathbf{s}_{t+1}))^2],$$

where the soft value function $V(\mathbf{s}_t) = \mathbb{E}_{\mathbf{a}_t \sim \pi(\cdot | \mathbf{s}_t)} [Q(\mathbf{s}_t, \mathbf{a}_t) - \alpha \log \pi(\mathbf{a}_t | \mathbf{s}_t)]$ is approximated using a Monte Carlo estimate. We refer the reader to (Haarnoja et al. 2018b) for more information about SAC.

Learning Feature Point State Representation

In this paper, we assume that the state \mathbf{s}_t is a stack of two consecutive images, that is $\mathbf{s}_t = [\mathbf{o}_t, \mathbf{o}_{t-1}]$. We represent the state \mathbf{s}_t as a collection of feature points extracted from input images $\mathbf{o}_t, \mathbf{o}_{t-1}$ with a differentiable feature point extractor. The extracted feature points are then used as the inputs of the actor and the critic heads of the SAC agent (see Fig. 1).

We define a feature point as a triplet (x_k, y_k, m_k) where x_k and y_k are the 2D coordinates of the feature point and $m_k \in (-1, 1)$ is a scalar feature which can, for example, encode the presence of the feature point in an image. Each input image \mathbf{o} is processed into a set of K feature points with a differentiable feature point bottleneck Φ :

$$\mathbf{x} = \Phi(\mathbf{o}) = [(x_1, y_1, m_1), \dots, (x_K, y_K, m_K)].$$

We use the vector $[\mathbf{x}_t, \mathbf{x}_t - \mathbf{x}_{t-1}]$ as the inputs of the actor and the critic heads, where $\mathbf{x}_t = \Phi(\mathbf{o}_t)$, $\mathbf{x}_{t-1} = \Phi(\mathbf{o}_{t-1})$

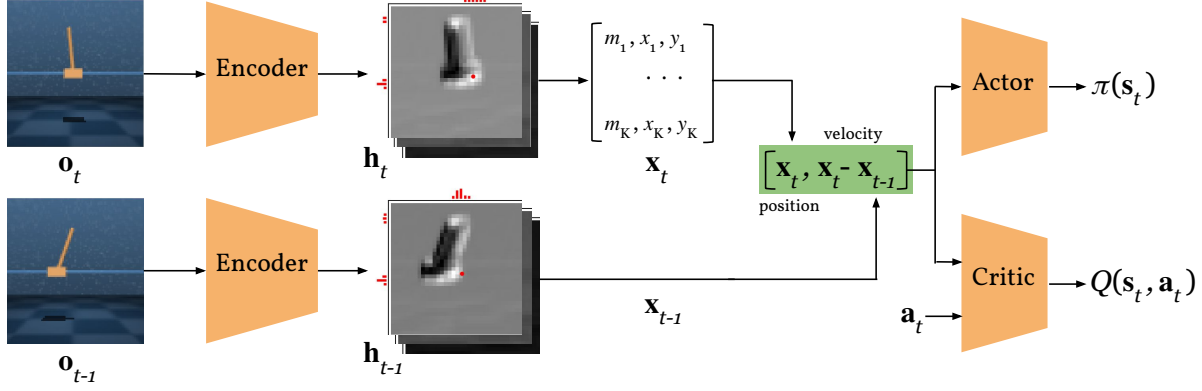


Figure 1: FPAC Architecture. At time-step t , a convolutional encoder is used to extract K feature maps \mathbf{h}_t from image observations \mathbf{o}_t . The features maps are considered as probability distributions of feature point locations and we extract K feature point locations and features $\mathbf{x}_t = [(m_1, x_1, y_1), \dots, (m_K, x_K, y_K)]$ from these K probability distributions \mathbf{h}_t (Equations (1) and (2)). We similarly compute \mathbf{h}_{t-1} and \mathbf{x}_{t-1} from \mathbf{o}_{t-1} and represent the current state as a concatenation of feature point position \mathbf{x}_t and feature point velocity $\mathbf{x}_t - \mathbf{x}_{t-1}$. This feature point state representation is given to the actor and critic networks. The feature points (that is, the weights of the convolutional encoder) are learned based on the gradients from the critic loss.

and $\mathbf{x}_t - \mathbf{x}_{t-1}$ encodes the feature point velocities. While we do not introduce explicit constraints to encourage temporal consistency of keypoints, this feature point velocity term could implicitly encourage that (See Fig. 12 in the Appendix for an ablation study of this velocity term).

We implement function $\mathbf{x} = \Phi(\mathbf{o})$ using the differentiable feature point bottleneck proposed by Levine et al. (2016). We use a convolutional network f to process image $\mathbf{o} \in \mathbb{R}^{H' \times W' \times C}$ into K feature maps of shape $H \times W$: $\mathbf{h} = f(\mathbf{o}) \in \mathbb{R}^{H \times W \times K}$. Let $h(x, y, k)$ denote the value of the k -th channel of \mathbf{h} at pixel (x, y) . The feature point coordinates (x_k, y_k) can be taken as the expected values of the pixel coordinates:

$$\begin{bmatrix} x_k \\ y_k \end{bmatrix} = \sum_{x=1}^W \sum_{y=1}^H \begin{bmatrix} x \\ y \end{bmatrix} p_k(x, y), \quad (1)$$

where the expectation is computed using distribution $p_k(x, y)$ produced using the softmax function:

$$p_k(x, y) = \frac{\exp(h(x, y, k))}{\sum_{x', y'} \exp(h(x', y', k))}.$$

The scalar feature m_k is computed as the tanh-activated mean value of the feature maps:

$$m_k = \tanh \left(\frac{1}{HW} \sum_{x=1}^W \sum_{y=1}^H h(x, y, k) \right). \quad (2)$$

In practice, we compute the coordinates (x_k, y_k) using a separable variant of (1) that is more efficient and also performed well in our experiments. For example, the x coordinate is computed as

$$x_k = \sum_{x=1}^W x p_k(x), \quad p_k(x) = \frac{\exp(\frac{1}{\beta} g(k, x))}{\sum_{x'} \exp(\frac{1}{\beta} g(k, x'))}, \quad (3)$$

where $g(k, x)$ is the mean-pooled value of $h(x, y, k)$ along dimension y :

$$g(k, x) = \frac{1}{H} \sum_{y=1}^H h(x, y, k).$$

The y coordinate is computed similarly. We use $\beta = 0.5$ in all our experiments.

The extracted feature points depend only on the weights of the convolutional encoder f . These weights are updated using the gradients of the critic loss so that the agent directly learns the feature point locations that are relevant for the RL task. We call our agent FPAC (feature point actor-critic) and its complete architecture is illustrated in Fig. 1. The PyTorch code for extracting feature points from convolutional feature maps is provided in Listing 1 in the Appendix.

Experimental Results

In this section, we evaluate our FPAC method on a set of image-based continuous control tasks from the DeepMind Control Suite (DMC) (Tassa et al. 2020). We first evaluate it on six tasks from the PlaNet benchmark (Hafner et al. 2019b) and further on eight additional tasks from the Dreamer benchmark (Hafner et al. 2019a). The tasks present qualitatively different learning challenges like the robot moving out of camera view (Cartpole), sparse rewards (Reacher, Ball in Cup), contacts between objects (Finger, Cheetah, Hopper, Walker), and a large number of joints (Cheetah, Walker). Following all prior works on the PlaNet benchmark (Yarats et al. 2019; Laskin, Srinivas, and Abbeel 2020; Yarats, Kostrikov, and Fergus 2021; Hafner et al. 2019b; Lee et al. 2020), we use different action repeat values for each task (listed in Table 2) and report the true environment steps (which is invariant to the action repeat parameter) in all our experiments. The Dreamer benchmark uses a constant action repeat of 2 steps on all tasks.

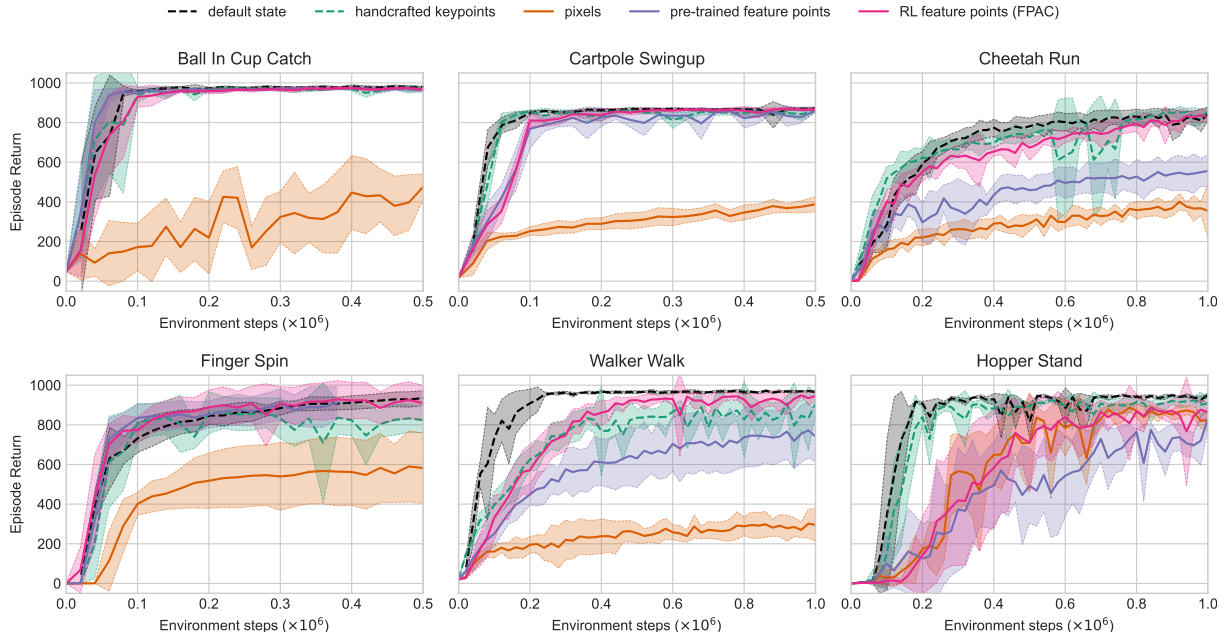


Figure 2: Evaluation of the efficacy of spatial coordinate representations on the PlaNet benchmark using the SAC algorithm. SAC with *handcrafted keypoints* (extracted from the simulator) performs almost as well as SAC with fine-tuned *default state* representations defined in DeepMind Control Suite, which suggests that 2D keypoints can be effective for state representation for control. While SAC from *pixels* is unable to learn, adding a feature point extraction bottleneck at the output of the convolutional encoder (*FPAC*) significantly improves performance. Using *pre-trained feature points* representations (pre-trained on extra data of 10k steps) performs well in simple tasks like Cartpole Swingup but does not perform as well in more challenging tasks like Cheetah Run, Walker Walk, and Hopper Stand. We plot the mean and standard deviation of 6 runs of all agents.

In the first experiment, we test whether spatial coordinate representations such as feature points can be an effective form of state representation for continuous control. Fig. 2 shows the learning curves of the different versions of the SAC agent:

- Agent that learns from raw *pixels*. This is a SAC agent that learns low-dimensional state representations from a stack of image observations with a convolutional encoder based on the critic loss (Haarnoja et al. 2018b). The only difference between this agent and our FPAC agent is the additional feature point bottleneck used in FPAC.
- Agent that uses the low-dimensional *default state* from DMC. This includes information like robot pose, joint positions, and joint velocities, and was fine-tuned separately for each task by Tassa et al. (2020).
- Agent that uses ground-truth locations of *handcrafted keypoints* that we manually extract from the simulator. We compute the keypoints by taking the 3D locations of the center of all objects in the environment and projecting them to the 2D pixel space of the default camera defined for all tasks. We found experimentally that relative positions of keypoints $\bar{x} = [(x_1 - \bar{x}, y_1 - \bar{y}, m_1), \dots, (x_K - \bar{x}, y_K - \bar{y}, m_K)]$, where \bar{x} and \bar{y} are the mean x and y coordinates of all K keypoints, generalize better than absolute positions with handcrafted keypoints and use this in our experiments. The first row of Fig. 3 shows examples of the handcrafted keypoints for all tasks in the

PlaNet benchmark. The Python code for extracting such pre-defined keypoints from the DeepMind Control Suite is provided in Listing 2 in the Appendix.

- Our *FPAC* agent which learns feature point representations of image observations from scratch using a convolutional feature point extractor updated using the critic loss.
- Agent that uses *pre-trained feature points*. We train a self-supervised feature points encoder from 10k images collected using a random policy. Pre-training is done similarly to (Jakab et al. 2018) by minimizing the reconstruction loss. The pre-trained feature points are used as the SAC inputs.

In Cheetah, Walker and Hopper tasks, for agents that use handcrafted keypoints, pre-trained feature points, and RL feature points (FPAC), we use additional information about the movements of the camera to translate the feature points in the past frame to the same coordinates as the current frame. We explain this in detail in the Appendix and also perform an ablation study of this use of extra camera information in Fig. 8.

One can see that the SAC algorithm can learn effectively from the handcrafted keypoints, with similar data-efficiency and asymptotic performance to that of learning from the default state, except for Walker Walk where it performs slightly worse. Note that the default state space is fine-tuned for each task such that RL algorithms can successfully learn from

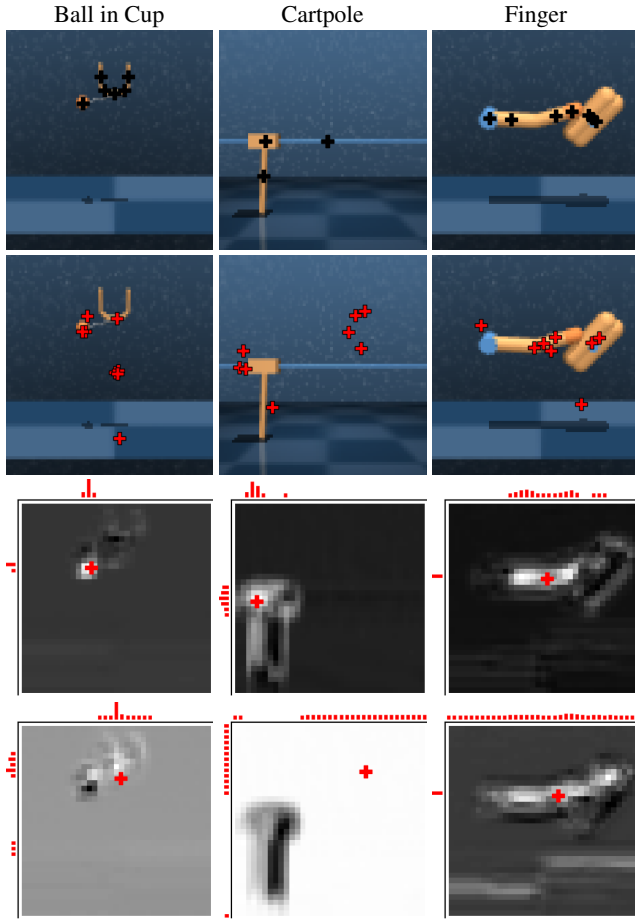


Figure 3: *Row 1*: Example frames from three tasks from the PlaNet benchmark. The black crosses represent the hand-crafted keypoints extracted from the simulator. *Row 2*: Feature points learned by FPAC with $K = 8$. *Rows 3 and 4*: Some feature maps $h(\cdot, \cdot, k)$ produced by the convolutional FPAC encoder along with the probability distributions of the feature point location (Equation 3). Brighter pixels indicate larger values. FPAC can learn to represent parts of an object (row 3), multiple objects (by activating the locations of multiple objects as, for example, in row 4 for Finger and Ball in Cup) or the background (row 4 for Cartpole).

them (Tassa et al. 2020) and the center locations of objects might not be the optimal spatial coordinate representation for continuous control in all tasks.

Our FPAC agent achieves similar data-efficiency and asymptotic performance as SAC from the handcrafted keypoints. FPAC performs worse in Cartpole and Hopper but better in Walker and Finger.

SAC from pixels performs poorly in all tasks except Hopper. FPAC performs significantly better by simply introducing an extra feature points bottleneck layer.

We observe that while SAC from pre-trained feature points performs better than SAC from pixels, it performs worse than FPAC in Cheetah and Walker. As the RL agent learns, it actively visits new states and the pre-trained feature

points fail to generalize to these new states (see Section in the Appendix for more details). FPAC directly learns the feature points relevant for the RL task and performs as well as SAC from the handcrafted keypoints and almost as well as SAC from the default state. These results suggest that end-to-end learning of feature points without any additional pre-training works at least as well as using a pre-trained feature point extractor on all considered tasks.

In Fig. 4, we compare our FPAC method to prior methods on the PlaNet benchmark:

- PlaNet (Hafner et al. 2019b) is a model-based RL algorithm that learns a latent dynamics model of the environment and computes actions by planning with the learned model.
- SLAC (Lee et al. 2020) also learns a latent dynamics model of the environment but learns policy and value functions on top of the latent representation, using the SAC algorithm.
- SAC-AE (Yarats et al. 2019) learns a regularized convolutional autoencoder jointly with the SAC algorithm.
- CURL (Laskin, Srinivas, and Abbeel 2020) learns a convolutional encoder using an unsupervised contrastive loss jointly with the SAC algorithm.
- DrQ (Yarats, Kostrikov, and Fergus 2021) averages the Q predictions and targets over different random shifts of image observations to train a convolutional encoder, based only on the critic loss.

All model-free algorithms considered in this paper (SAC from pixels, SAC-AE, CURL, DrQ, and FPAC) use the same reinforcement learning algorithm (SAC) and base network architectures: a four-layer convolutional encoder (with 32 channels, kernel size 3, and a stride of 2 on the first layer) and shallow feedforward actor-critic networks. All hyperparameters used in our experiments are listed in Table 2 in the Appendix.

FPAC performs competitively to the state-of-the-art DrQ method and better than all the other methods on most tasks. FPAC outperforms all methods in the Ball in Cup Catch and Cheetah Run tasks.

To further test the robustness of FPAC, we compare it to prior methods on eight additional tasks from the Dreamer benchmark in Fig. 5. FPAC performs well on all tasks, with sample-efficiency and asymptotic performance comparable to the state-of-the-art DrQ and Dreamer methods. The 14 different tasks we considered in our experiments have a different number of objects and object dynamics. FPAC can learn feature points to represent them, to perform robustly well on all tasks.

We plot the feature points learned by FPAC along with a few selected feature maps produced by the convolutional encoder in Fig. 3. FPAC learns to represent the locations of the relevant objects in the scene. We observe that FPAC also learns feature points to represent multiple objects that are relevant to the control task (see Fig. 6). The feature point representations learned by neural networks do not typically correspond to explainable visual cues. Learning more human interpretable feature points is an important topic for future research.

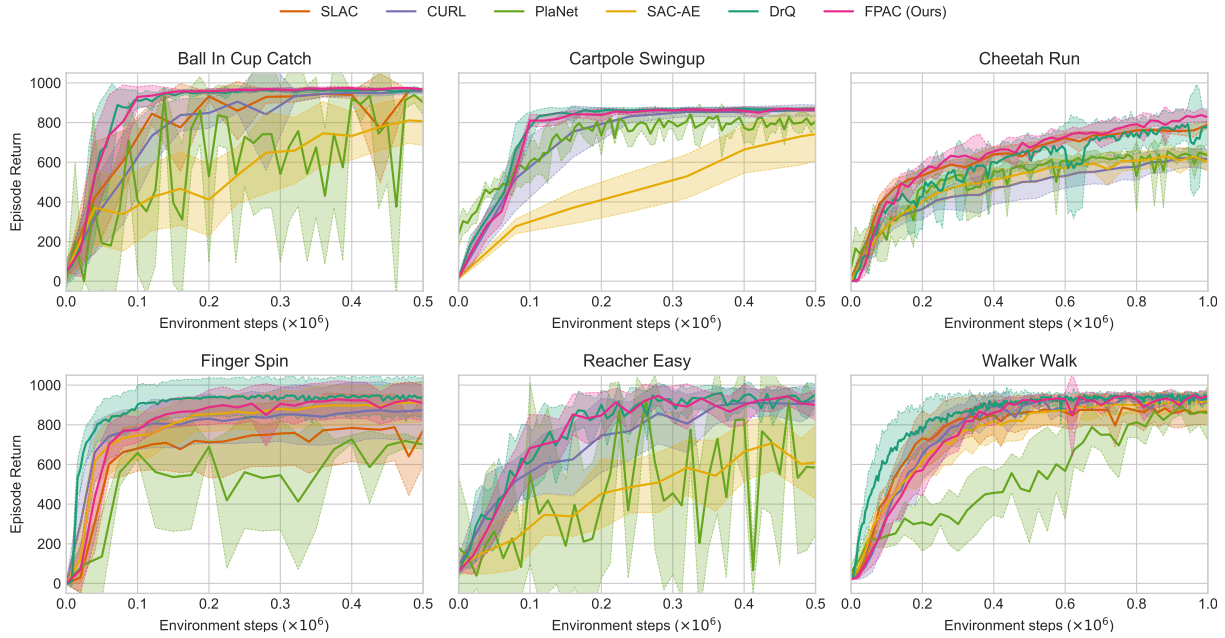


Figure 4: Comparison of FPAC to prior methods on the PlaNet benchmark. FPAC performs competitively to the state-of-the-art DrQ, CURL and SLAC methods. We plot the mean and standard deviation of 10 runs of all agents. Results of other methods taken from (Yarats, Kostrikov, and Fergus 2021).

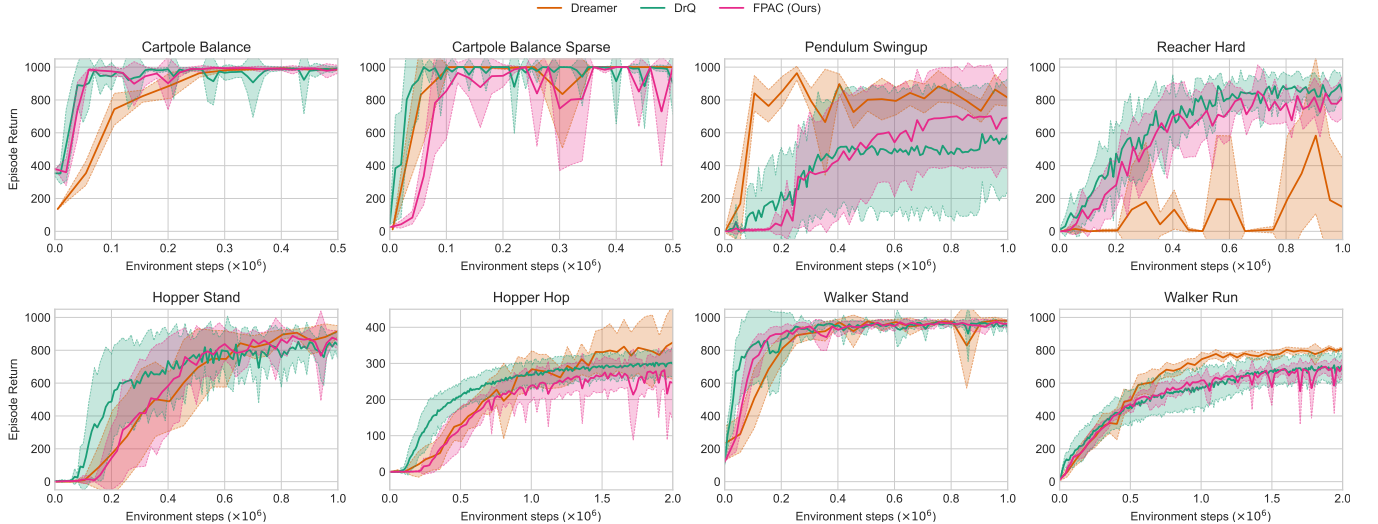


Figure 5: Comparison of FPAC to prior methods on eight additional tasks from the Dreamer benchmark. FPAC performs competitively to the state-of-the-art DrQ and Dreamer methods. We plot the mean and standard deviation of 10 runs of all agents. Results of other methods taken from (Yarats, Kostrikov, and Fergus 2021).

We analyze the robustness of FPAC to the number of learned feature points, which is a hyperparameter. The results of our experiments are shown in Fig. 7 in the Appendix. We observe that FPAC is robust to the number of feature points and performs similarly well on all tasks with 8, 16, 24, 32, or 64 feature points, except Reacher Easy where FPAC performs worse with 8 feature points. So, given enough capacity, FPAC is robust and performs well across all tasks.

We further analyze the design choices and robustness of our FPAC agent in detail in the Appendix. We observe that our FPAC method is robust to design and implementation choices such as the use of scalar feature m_k , use of feature point velocity term, use of relative spatial coordinates, and the use of separable spatial softmax implementation.

Our FPAC method is easy to implement and fast to run. We measure an overall training time of 70 minutes 41 sec-

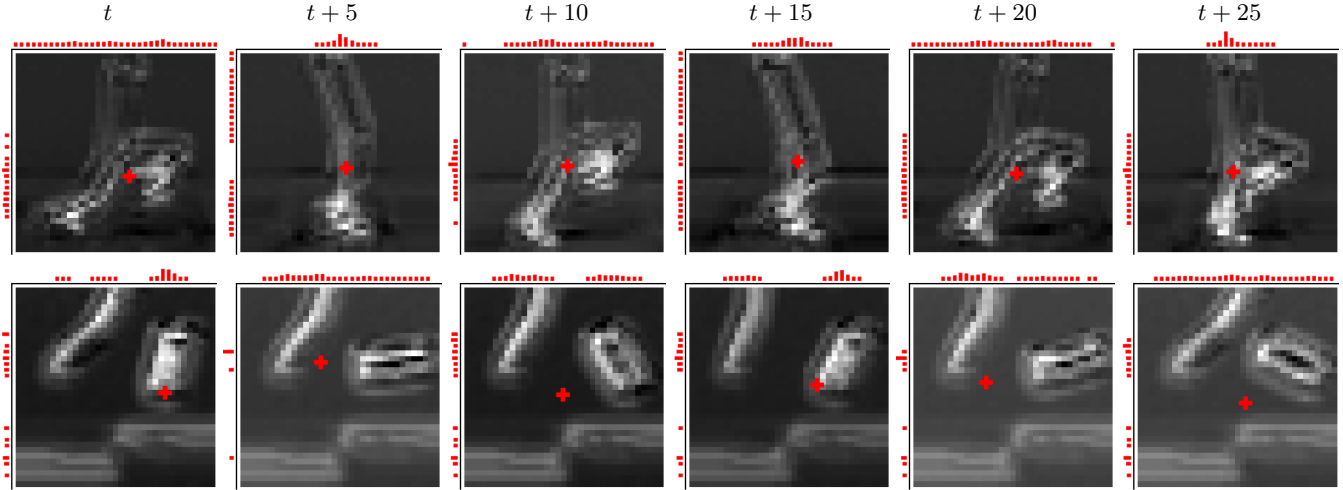


Figure 6: Dynamics of feature maps of keypoints that learn to represent multiple objects. Brighter pixels indicate larger values. *Row 1*: a keypoint that tracks the front and back legs in the Walker Walk task. *Row 2*: a keypoint that tracks the finger and rotatable body, relative to the floor, in the Finger Spin task.

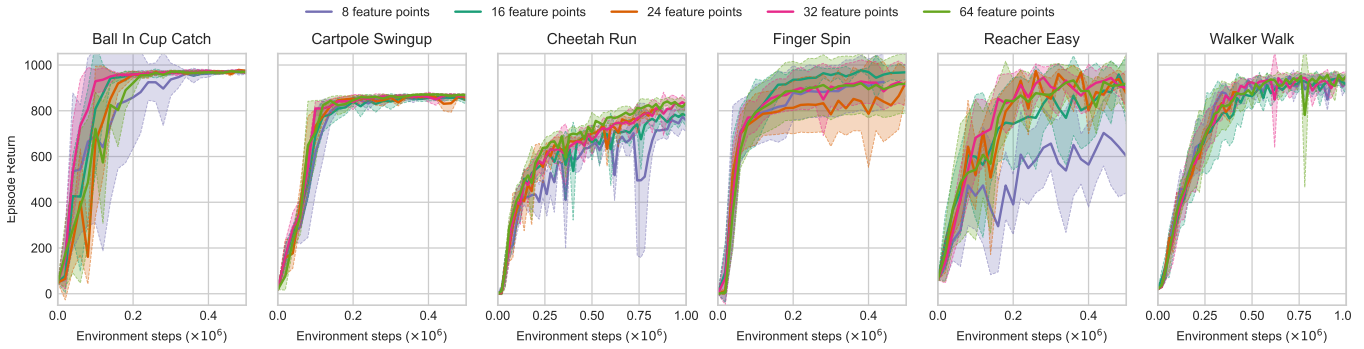


Figure 7: FPAC learns robustly with a different number K of extracted feature points. FPAC achieves similar asymptotic performance on all tasks, except Reacher Easy. We plot the mean and standard deviation of 6 runs of all agents.

onds to train a SAC from pixels agent and 76 minutes 56 seconds to train our FPAC agent for 500 episodes on the Cartpole Swingup task. We report an average of 10 runs on an NVIDIA V100 GPU. The only difference between the SAC from pixels agent and our FPAC agent is the additional feature point bottleneck used in FPAC. The additional feature point bottleneck makes our approach only negligibly slower (while performing significantly better) than SAC from pixels (which does not learn well).

Conclusion

We demonstrate that it is possible to directly learn feature points that are relevant for RL from images, without any additional supervision. Our FPAC method, which only adds a simple feature points bottleneck, is easy to implement and fast to run. We demonstrate that FPAC performs competitively to the state-of-the-art methods on the PlaNet and Dreamer benchmarks. FPAC can learn feature points from scratch, even in tasks with sparse rewards, to nearly match the performance of SAC learning from low-dimensional rep-

resentations. We observe that feature points learned end-to-end, from scratch, work at least as well as feature points learned with pre-training. FPAC is robust to the choice of hyperparameters and can perform robustly across tasks with a different number of objects and different object dynamics. The code to reproduce our experiments is provided in the supplementary material. Potential lines of future work include: (i) learning feature point dynamics models that can be used to generate additional data to train actor-critic networks, and (ii) learning 3D feature points from monocular images or multiple views.

References

Cabi, S.; Colmenarejo, S. G.; Novikov, A.; Konyushkova, K.; Reed, S.; Jeong, R.; Zolna, K.; Aytar, Y.; Budden, D.; Vercerik, M.; et al. 2020. Scaling data-driven robotics with reward sketching and batch reinforcement learning. *Robotics: Science and Systems*.

Finn, C.; Tan, X. Y.; Duan, Y.; Darrell, T.; Levine, S.; and Abbeel, P. 2016. Deep spatial autoencoders for visuomo-

tor learning. In *2016 IEEE International Conference on Robotics and Automation (ICRA)*, 512–519. IEEE.

Gopalakrishnan, A.; van Steenkiste, S.; and Schmidhuber, J. 2021. Unsupervised Object Keypoint Learning using Local Spatial Predictability. In *International Conference on Learning Representations*.

Ha, D.; and Schmidhuber, J. 2018. Recurrent world models facilitate policy evolution. In *Advances in Neural Information Processing Systems*, 2455–2467.

Haarnoja, T.; Zhou, A.; Abbeel, P.; and Levine, S. 2018a. Soft actor-critic: Off-policy maximum entropy deep reinforcement learning with a stochastic actor. In *International Conference on Machine Learning*, 1861–1870.

Haarnoja, T.; Zhou, A.; Hartikainen, K.; Tucker, G.; Ha, S.; Tan, J.; Kumar, V.; Zhu, H.; Gupta, A.; Abbeel, P.; et al. 2018b. Soft actor-critic algorithms and applications. *arXiv preprint arXiv:1812.05905*.

Hafner, D.; Lillicrap, T.; Ba, J.; and Norouzi, M. 2019a. Dream to Control: Learning Behaviors by Latent Imagination. In *International Conference on Learning Representations*.

Hafner, D.; Lillicrap, T.; Fischer, I.; Villegas, R.; Ha, D.; Lee, H.; and Davidson, J. 2019b. Learning latent dynamics for planning from pixels. In *International Conference on Machine Learning*, 2555–2565.

Higgins, I.; Pal, A.; Rusu, A.; Matthey, L.; Burgess, C.; Pritzel, A.; Botvinick, M.; Blundell, C.; and Lerchner, A. 2017. DARLA: Improving Zero-Shot Transfer in Reinforcement Learning. In *International Conference on Machine Learning*, 1480–1490.

Jakab, T.; Gupta, A.; Bilen, H.; and Vedaldi, A. 2018. Unsupervised Learning of Object Landmarks through Conditional Image Generation. In *Advances in Neural Information Processing Systems*, volume 31.

Kendall, A.; Hawke, J.; Janz, D.; Mazur, P.; Reda, D.; Allen, J.-M.; Lam, V.-D.; Bewley, A.; and Shah, A. 2019. Learning to drive in a day. In *IEEE International Conference on Robotics and Automation*, 8248–8254.

Kulkarni, T. D.; Gupta, A.; Ionescu, C.; Borgeaud, S.; Reynolds, M.; Zisserman, A.; and Mnih, V. 2019. Unsupervised learning of object keypoints for perception and control. In *Advances in Neural Information Processing Systems*, volume 32, 10724–10734.

Lange, S.; and Riedmiller, M. A. 2010. Deep learning of visual control policies. In *ESANN*.

Laskin, M.; Lee, K.; Stooke, A.; Pinto, L.; Abbeel, P.; and Srinivas, A. 2020. Reinforcement Learning with Augmented Data. In *Advances in Neural Information Processing Systems*, volume 33.

Laskin, M.; Srinivas, A.; and Abbeel, P. 2020. CURL: Contrastive Unsupervised Representations for Reinforcement Learning. In *International Conference on Machine Learning*.

Lee, A.; Nagabandi, A.; Abbeel, P.; and Levine, S. 2020. Stochastic Latent Actor-Critic: Deep Reinforcement Learning with a Latent Variable Model. In *Advances in Neural Information Processing Systems*, volume 33.

Levine, S.; Finn, C.; Darrell, T.; and Abbeel, P. 2016. End-to-end training of deep visuomotor policies. *The Journal of Machine Learning Research*, 17(1): 1334–1373.

Manuelli, L.; Li, Y.; Florence, P.; and Tedrake, R. 2020. Keypoints into the Future: Self-Supervised Correspondence in Model-Based Reinforcement Learning. In *Conference on Robot Learning*.

Minderer, M.; Sun, C.; Villegas, R.; Cole, F.; Murphy, K.; and Lee, H. 2019. Unsupervised learning of object structure and dynamics from videos. In *Advances in Neural Information Processing Systems*.

Nair, A. V.; Pong, V.; Dalal, M.; Bahl, S.; Lin, S.; and Levine, S. 2018. Visual reinforcement learning with imagined goals. In *Advances in Neural Information Processing Systems*, 9191–9200.

Ramachandran, P.; Zoph, B.; and Le, Q. V. 2017. Searching for activation functions. *arXiv preprint arXiv:1710.05941*.

Shelhamer, E.; Mahmoudieh, P.; Argus, M.; and Darrell, T. 2016. Loss is its own reward: Self-supervision for reinforcement learning. *arXiv preprint arXiv:1612.07307*.

Singh, A.; Yang, L.; Hartikainen, K.; Finn, C.; and Levine, S. 2019. End-to-End Robotic Reinforcement Learning without Reward Engineering. *Robotics: Science and Systems*.

Tassa, Y.; Tunyasuvunakool, S.; Muldal, A.; Doron, Y.; Trochim, P.; Liu, S.; Bohez, S.; Merel, J.; Erez, T.; Lillicrap, T.; et al. 2020. dm_control: Software and tasks for continuous control. *arXiv preprint arXiv:2006.12983*.

Thewlis, J.; Albanie, S.; Bilen, H.; and Vedaldi, A. 2019. Unsupervised learning of landmarks by descriptor vector exchange. In *IEEE International Conference on Computer Vision*, 6361–6371.

Thewlis, J.; Bilen, H.; and Vedaldi, A. 2017. Unsupervised learning of object landmarks by factorized spatial embeddings. In *IEEE International Conference on Computer Vision*, 5916–5925.

Viitala, A.; Boney, R.; Zhao, Y.; Ilin, A.; and Kannala, J. 2020. Learning to Drive (L2D) as a Low-Cost Benchmark for Real-World Reinforcement Learning. *arXiv preprint arXiv:2008.00715*.

Yarats, D.; Kostrikov, I.; and Fergus, R. 2021. Image Augmentation Is All You Need: Regularizing Deep Reinforcement Learning from Pixels. In *International Conference on Learning Representations*.

Yarats, D.; Zhang, A.; Kostrikov, I.; Amos, B.; Pineau, J.; and Fergus, R. 2019. Improving sample efficiency in model-free reinforcement learning from images. *arXiv preprint arXiv:1910.01741*.

Zhang, Y.; Guo, Y.; Jin, Y.; Luo, Y.; He, Z.; and Lee, H. 2018. Unsupervised discovery of object landmarks as structural representations. In *IEEE Conference on Computer Vision and Pattern Recognition*, 2694–2703.

Zhu, H.; Yu, J.; Gupta, A.; Shah, D.; Hartikainen, K.; Singh, A.; Kumar, V.; and Levine, S. 2019. The Ingredients of Real World Robotic Reinforcement Learning. In *International Conference on Learning Representations*.

Ablation studies

Data-efficiency and asymptotic performance of FPAC on PlaNet benchmark

Following prior works, we compare the data-efficiency and asymptotic performance of FPAC based on returns on 100k and 500k steps of the PlaNet benchmark in Table 1. FPAC performs competitively to the state-of-the-art methods.

Use of camera movement information

In Cheetah, Hopper, and Walker tasks, we use the movement of the camera to translate the feature points in the past frame to the same coordinates as the current frame. We measure the impact of using this extra camera information in Fig. 8. We observe that this is significantly helpful in Cheetah Run but does not have any impact in Walker Walk. We hypothesize that this is due to the fact that the “cheetah” always stays in the center of the image and the only motion cue in these observations is the lightly colored checkboard pattern on the floor. Use of camera movement allows the agent to separate the movements of the robot and the camera and only use what is relevant for the task (that is, only the robot movement). Note that this is also possible in real-world applications by using computer vision approaches to track the movement of the camera. Also, we use this information only in the agents that use feature point representations because inserting this information to other agents is not trivial.

Generalization of pre-trained feature points

In our experiments, we observed that pre-trained feature points perform similar to FPAC on the simpler tasks (Ball in Cup, Cartpole, Finger, Reacher) and significantly worse on Cheetah and Walker (see Fig. 2). We investigate this by looking at the predictions of the pre-trained encoder as RL training progresses. We plot some predictions in Fig. 9. We observe that as the RL agent learns, it visits new states that are out-of-distribution of the pre-trained encoder and the pre-trained feature points fail to generalize well on these states. This significantly decreases the data-efficiency and asymptotic performance of the RL agent.

For further analysis, we plot the y-coordinate of the torso of the cheetah throughout a training run in Fig. 10. We can observe that the distribution of this measurement is narrow in the initial random exploration phase of training. After training on more steps, exploration by the RL agent leads to upside down flipping of the cheetah. This is denoted by a jump from higher to lower y-coordinate value in Fig. 10. As we show in Fig. 9, the pre-trained encoder does not make accurate feature point predictions in these states and subsequently the RL agent with pre-trained feature points fails to recover and continues to flip even if we train it for longer. In contrast, our FPAC agent with end-to-end training also explores flipping in the initial stages of training but quickly learns to recover (as the feature points encoder learns to extract the right feature points on newly visited states) and run forward efficiently.

While it might be possible to tune the pre-training so that it generalizes well, FPAC learns relevant feature points from

scratch, in an end-to-end manner, to match the learning performance of SAC from handcrafted keypoints and performs competitive to the state-of-the-art methods on PlaNet and Dreamer benchmarks.

Impact of scalar feature

We measure the impact of scalar feature m_k on the learning performance of FPAC in Fig. 11. Use of the scalar feature has a significant impact in the Ball in Cup Catch task but only a minor impact on other tasks.

Impact of feature point velocity term

We measure the impact of the feature point velocity term in Fig. 12. We observe that while FPAC is able to learn most tasks reasonably well even without the velocity term, FPAC with the velocity term consistently performs better.

Impact of separable spatial softmax

The feature point coordinates can be computed as the expected values of pixel coordinates, after a spatial softmax operation (Levine et al. 2016) on the convolutional feature maps (1). We refer to this version as *FPAC, spatial softmax*. In practice, we use a separable variant that computes each coordinate separately (3). We refer to this version as *FPAC, separable variant*. We compare the RL performance of the spatial softmax version against the separable variant in Fig. 13. We observe that both perform similarly and the separable variant performs slightly better than the spatial softmax version in some tasks.

The separable variant is also computationally more efficient than the spatial softmax version. We benchmark both versions on an NVIDIA GTX 1080 Ti GPU. We perform 100k calls to both functions using a batch of $128 \times 32 \times 35 \times 35$ convolutional feature maps and measure the average time required for each operation. The spatial softmax version takes 2.8 ms, with the majority of the time spent on the 2D softmax operation which takes 1.8 ms and then the 2D expectation operation for each coordinate takes 0.5 ms. The separable variant only takes 1.1 ms where the mean pooling, 1D softmax, and 1D expectation operation for each coordinate takes 0.55 ms.

Impact of relative feature points

We measure the impact of using absolute vs relative feature point coordinates on the learning performance of FPAC in Fig. 14. Use of the relative feature points only has a significant impact in the Ball in Cup Catch task. Use of absolute feature points generalizes well to all tasks.

Network architecture and hyperparameters

Similar to prior works, our convolutional encoder consists of four convolutional layers with 32 channels, 3×3 kernels and a stride of 2 on the first layer. These convolutional layers reduce the $3 \times 84 \times 84$ observations to $32 \times 35 \times 35$ feature maps and we additionally use a 1×1 convolutional layer to project these 32 feature maps to K feature maps (to compute locations and features for K feature points). For our

500k step scores	FPAC	DrQ	SLAC	CURL	SAC-AE	PlaNet
Ball In Cup, Catch	966 ± 6	963 ± 9	959 ± 4	958 ± 13	810 ± 121	939 ± 43
Cartpole, Swingup	866 ± 8	868 ± 10	-	861 ± 30	730 ± 152	787 ± 46
Cheetah, Run	673 ± 64	660 ± 96	629 ± 74	500 ± 91	544 ± 50	568 ± 21
Finger, Spin	909 ± 89	938 ± 103	771 ± 203	874 ± 151	914 ± 107	718 ± 40
Reacher, Easy	900 ± 75	942 ± 71	-	904 ± 94	601 ± 135	588 ± 471
Walker, Walk	924 ± 17	921 ± 45	865 ± 97	906 ± 56	858 ± 82	478 ± 164
100k step scores						
Ball In Cup, Catch	929 ± 50	913 ± 53	607 ± 173	772 ± 241	338 ± 196	710 ± 217
Cartpole, Swingup	810 ± 30	759 ± 92	-	592 ± 170	276 ± 38	563 ± 73
Cheetah, Run	401 ± 56	344 ± 67	391 ± 47*	307 ± 48	252 ± 173	165 ± 123
Finger, Spin	783 ± 64	901 ± 104	680 ± 130	779 ± 108	747 ± 130	560 ± 77
Reacher, Easy	682 ± 170	601 ± 213	-	517 ± 113	225 ± 164	82 ± 174
Walker, Walk	332 ± 112	612 ± 164	428 ± 74	344 ± 132	395 ± 58	221 ± 43

Table 1: Comparison of our FPAC method to other methods, on 100k and 500k steps of the PlaNet benchmark. We report the mean and standard deviation of 10 runs on each task. Our FPAC method performs competitively with the state-of-the-art methods. Results of other methods taken from (Yarats, Kostrikov, and Fergus 2021). * SLAC uses extra 100k exploration steps which are not counted in the step count while others agents only use 1k exploration steps which are included in the step count.

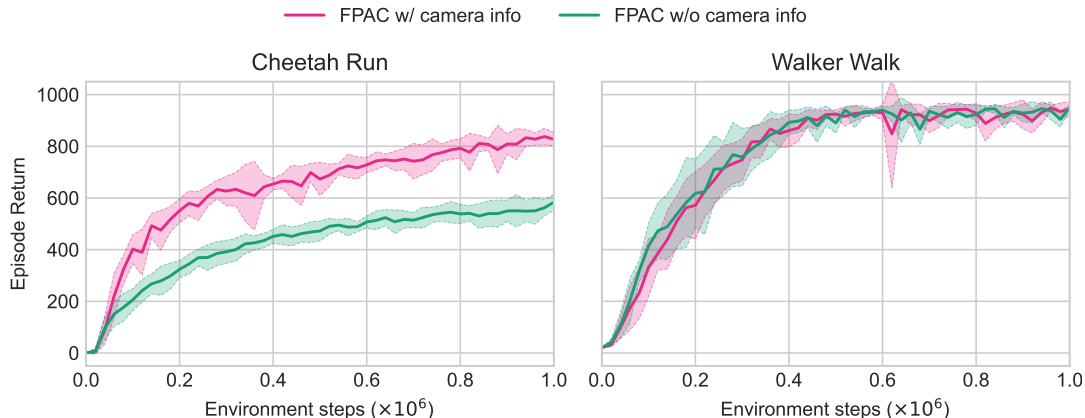


Figure 8: Ablation study on the use of camera movement information. We observe that the camera movement information significantly helps in Cheetah Run while it doesn't impact the performance in Walker Walk.

actor and critic networks, we use MLPs with 2 hidden layers and 1024 hidden units in each layer. We use the Swish non-linearity (Ramachandran, Zoph, and Le 2017) in all our networks. All hyperparameters used in our experiments are listed in Table 2.

Supporting code

We provide the PyTorch code for computing feature points from convolutional feature maps in Listing 1 and the Python code for extracting handcrafted keypoints from DeepMind control suite in Listing 2.



Figure 9: Failure of pre-trained feature points (learned using self-supervised training) on Cheetah Run. *Left*: self-supervised training learns to represent all relevant parts of the cheetah robot. *Middle and Right*: pre-trained feature point predictions fail to generalize to unseen observations. As an RL agent learns, it actively visits new states and it is crucial to use representations that generalize to new states or to continuously learn them.

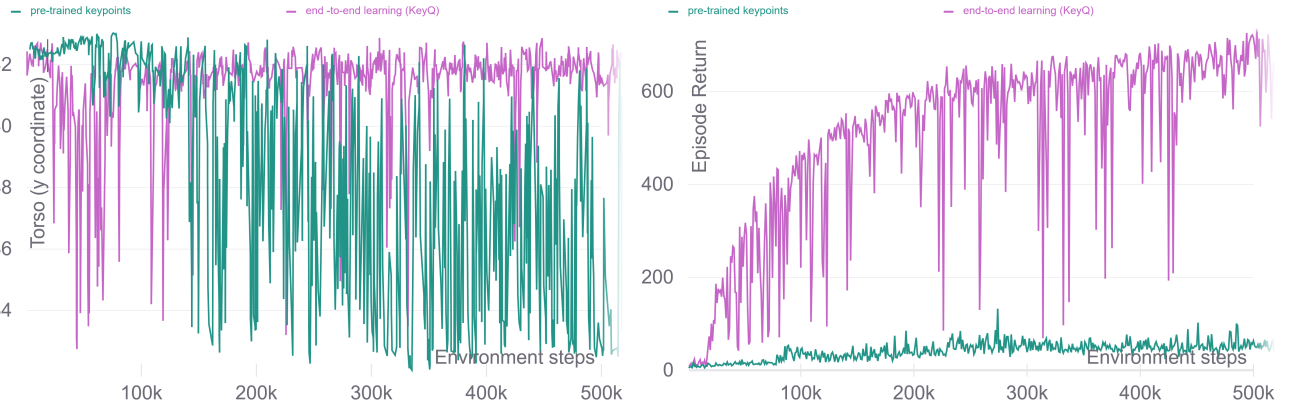


Figure 10: Analysis on the failure of pre-trained feature points (learned using self-supervised training) on Cheetah Run. *Left*: We plot the y-coordinate of the torso of the cheetah throughout two training runs on the Cheetah Run task. Note that we plot the position in pixels coordinates of 84×84 image observations. A high to low drop in this value indicates that the cheetah has flipped upside down. We can observe that the agent with pre-trained feature points continues to flip the cheetah and never recovers from it but the end-to-end learning agent quickly recovers from it and learns to solve the task. *Right*: We plot the returns of the same agents. As evident from plot of the torso position, we can observe that the agent with pre-trained feature points fails to progress on the task.

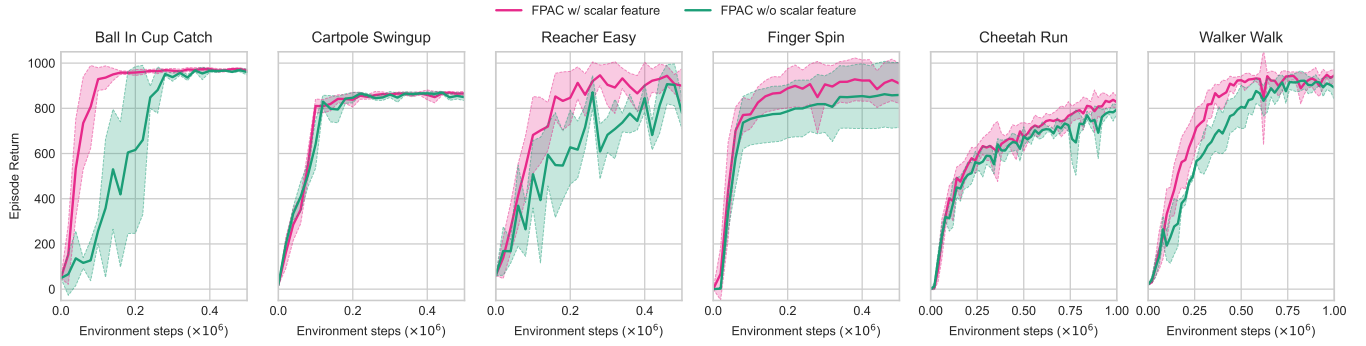


Figure 11: Impact of feature point scale feature m_t on learning performance of FPAC.

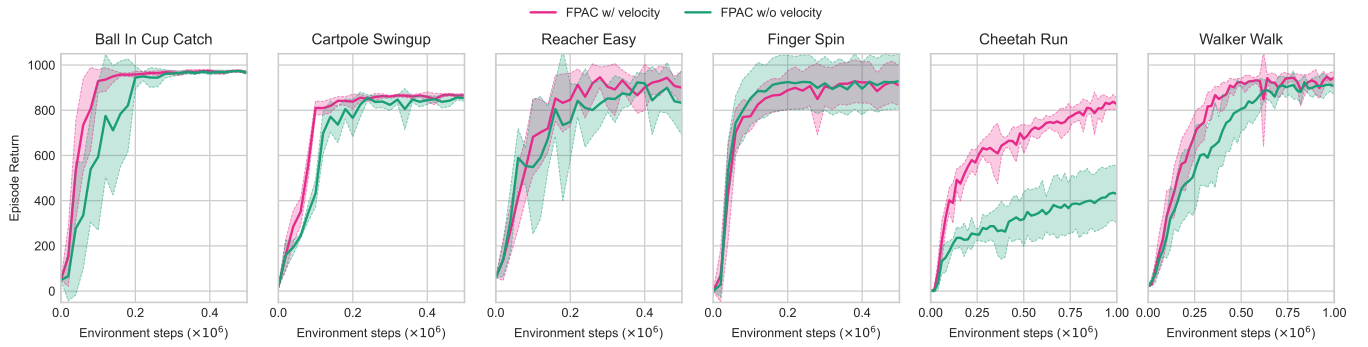


Figure 12: Impact of feature point velocity term on learning performance of FPAC.

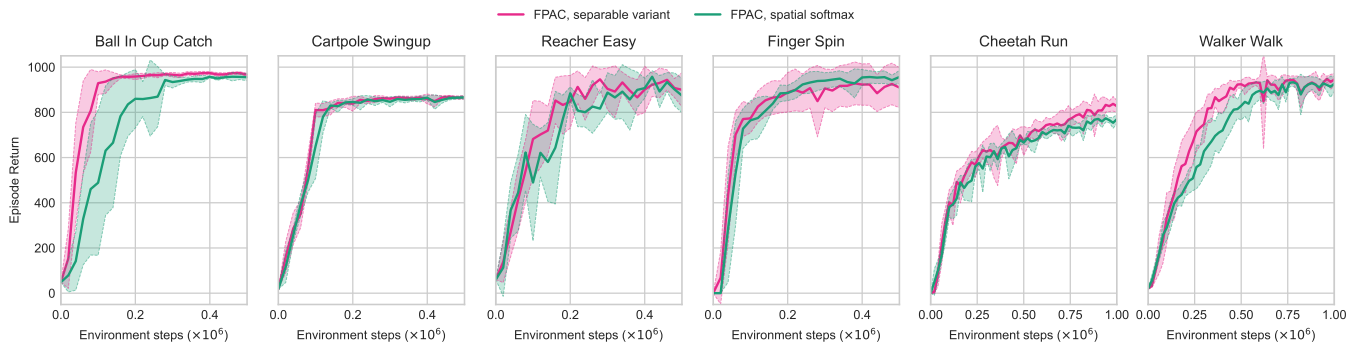


Figure 13: Impact of separable spatial softmax implementation on learning performance of FPAC.

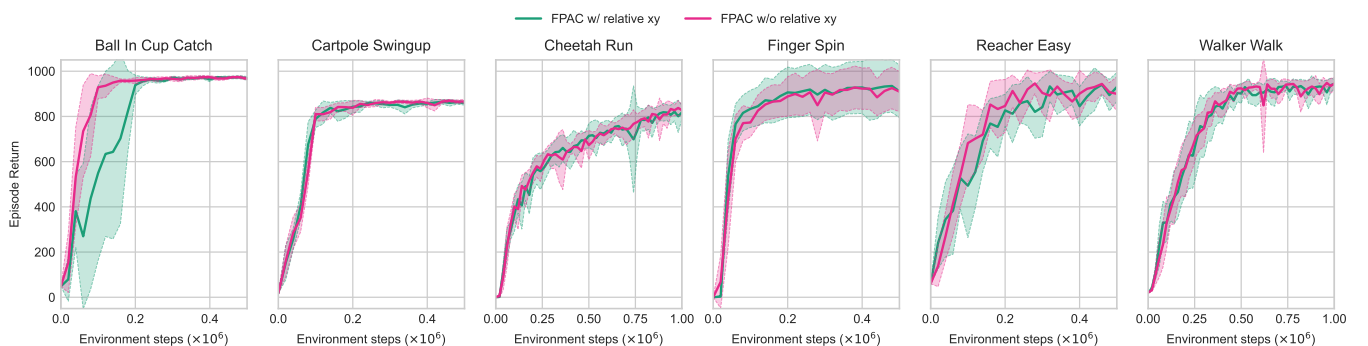


Figure 14: Impact of relative feature points on learning performance of FPAC.

Table 2: Hyperparameters used in our experiments. The hyperparameters are common across all tasks, except the initial learning rate for Reacher and the action repeat values defined in the PlaNet benchmark.

Hyperparameter	Value
Observation size	(84, 84)
Action repeat (PlaNet)	2, Finger and Walker 8, Cartpole 4, otherwise
Replay buffer capacity	100000
Batch size	128
Learning rate	1e-3, first 200k steps of Reacher 3e-4, otherwise
Optimizer	Adam
Evaluation episodes	10
Discount factor γ	0.99
Initial random steps	1000
Initial temperature	0.1
Target update rate τ	0.01
Target update frequency	2
Actor update frequency	2
Frame stack	2
MLP hidden layers	2
MLP hidden units	1024
Non-linearity	Swish
Number of feature points	32
Feature point temperature	0.5

Listing 1: PyTorch code for computing feature points from convolutional feature maps

```

1  def compute_feature_points(feature_maps, temperature=1):
2      """
3          Compute feature point locations and features from
4          feature_maps of shape [batch_size, num_points, H, W]
5      """
6      device = feature_maps.device
7      maps_size = feature_maps.size(-1)
8      coords = torch.linspace(-1, 1, maps_size, device=device)
9
10     def compute_coord(other_axis):
11         # Mean pooling
12         logits_1d = feature_maps.mean(other_axis)
13         # Compute feature point probabilities
14         key_probs = F.softmax(logits_1d / temperature, dim=-1)
15         # Compute expectation of the distribution
16         mean = (coords[None, None, :] * key_probs).sum(-1)
17         return mean
18
19     # Compute feature point locations
20     xs = compute_coord(-2)
21     ys = compute_coord(-1)
22     # Compute scalar feature
23     ps = torch.tanh(torch.flatten(feature_maps, -2, -1).mean(-1))
24     return xs, ys, ps

```

Listing 2: Python code for extracting handcrafted keypoints from DeepMind Control Suite

```
1  from dm_control.mujoco.engine import Camera
2
3  def gt_keypoints(env: dm_env.Environment):
4      # Load camera instance to get camera matrix
5      camera = Camera(env.physics, height=84, width=84, camera_id=0)
6      # Fetch xyz location of the center of all objects
7      xyz = env.physics.named.data.geom_xpos[1:]
8      # Add extra column of 1s
9      xyzs = np.ones((xyz.shape[0], xyz.shape[1]+1))
10     xyzs[:, :xyz.shape[1]] = xyz
11     # Project 3D locations to 2D pixels coordinates
12     xs, ys, s = camera.matrix.dot(xyzs.T)
13     # Return 2D keypoints
14     return xs/s, ys/s
```
